Observation of nuclear gamma resonance with superconducting tunnel junction detectors

M. G. Kozin,[1,a] I. L. Romashkina,[1] L. V. Filippenko,[2] and V. P. Koshelets[2]
[1]*Skobeltsyn Institute of Nuclear Physics (MSU SINP), Lomonosov Moscow State University, 1(2), Leninskie gory, GSP-1, Moscow 119991, Russian Federation*
[2]*Kotel'nikov Institute of Radio Engineering and Electronics of Russian Academy of Sciences, Mokhovaya 11-7, Moscow, 125009, Russian Federation*

(Received 7 August 2015; accepted 8 February 2016; published online 16 February 2016)

Nb-based superconducting tunnel junction detectors have been used for the registration of electrons following a nuclear gamma resonance (Mössbauer effect). Electrons were produced by a RhFe scatterer under irradiation by the ^{57}Co(Rh) Mössbauer source. This observation demonstrates the role which can be played by superconducting tunnel junction detectors in the field of conversion electron Mössbauer spectroscopy and other types of electron spectroscopy. [http://dx.doi.org/10.1063/1.4942429]

I. INTRODUCTION

New applications of low temperature detectors (LTDs) for the registration of electromagnetic radiation or particles are important because they usually demonstrate the superiority of LTDs over other solid state or gas detectors. A comprehensive review of the LTDs is presented in a book,[1] one chapter of which is devoted to the superconducting tunnel junction (STJ) detectors.[2] The application of STJs for radiation detection started from the registration of tunneling current pulses from Sn STJ bombarded by alpha particles.[3] The theory and applications of STJ detectors for photon detection have been considered by Friedrich.[4] The development of STJ detectors along with other types of LTDs gave an impulse to the development of nonequilibrium superconductivity and issues concerning the relaxation of excitations in superconducting materials used for the detector design. The idea of combining STJ with the Mössbauer spectroscopy came from the fact that Ta is the material of choice in modern STJ detectors and at the same time it almost entirely consists of the Mössbauer isotope ^{181}Ta. Taking this into account we put forward the idea of using a Ta absorber in the STJ detector in order to develop a resonance cryogenic detector for ^{181}Ta Mössbauer spectroscopy.[5] The coupling of STJ detectors with nuclear gamma resonance (NGR) spectroscopy may also be of interest in some other fields where the NGR can be applied.

Previously we demonstrated that it is possible to detect Fe K_α and K_β X-rays (6.40 and 7.06 keV) as well as 14.42 keV γ-rays from the ^{57}Co(Rh) Mössbauer source by means of a Nb based STJ detector.[6] In the present study we observed the Mössbauer effect in the scattering geometry with the ^{57}Co(Rh) Mössbauer source, RhFe scatterer and a Nb based STJ detector by registering electrons accompanying the NGR.

The main motivation for the development of X-ray detectors in the beginning of the STJ research was to obtain a high energy resolution, which however was not achieved experimentally. Later on, various aspects of X-ray registration by the STJ attracted closer attention. An X-ray detector operates as a detector of photoelectrons knocked out by an X-ray from the inner shells of absorber atoms (predominantly L-shell in the case of a Nb absorber and 5.89 keV Mn K_α X-ray from the benchmark ^{55}Fe source). However, STJs have not been used for the registration of electrons impinging detector from outside as far as we know. The only case of this kind is Ref. 7, where a small focused beam of 4 keV electrons in a low-temperature scanning electron microscope was

[a]Author to whom correspondence should be addressed. E-mail: kozin@srd.sinp.msu.ru

TABLE I. Photons and electrons produced after decay of excited state of the ^{57}Fe nucleus (data from Refs. 8 and 10).

Radiation		Energy, keV	Intensity per decay
γ-rays		14.42	0.09
X-rays	K_α	6.40	0.28
	K_β	7.06	
Conversion electrons	K	7.3	0.71
	L	13.6	0.07
	M	14.3	0.01
Auger electrons	K-LL	5.5	0.6

used to simulate 6 keV X-rays in order to investigate the detector response non-uniformity over the detector surface.

It is well known that the registration of the Mössbauer effect by secondary radiation (γ-, X-rays and conversion electrons) has certain advantages over the registration of primary radiation attenuation. These advantages are due to the possibility of obtaining a better signal to noise ratio and to probe different depths for different kinds of registered radiation. Various applications of the Mössbauer scattering techniques were thoroughly surveyed by Wagner.[8] More specifically, the conversion electron Mössbauer spectroscopy (CEMS) and its applications to surface layer analysis were considered in Ref. 9. Our previous[6] and present studies show that the Nb based STJ detectors can be used (at least, in principle) for all kinds of secondary radiation in the Mössbauer spectroscopy with the ^{57}Fe isotope.

The conversion coefficient of the ^{57}Fe Mössbauer transition is about nine. This means that there is an emission of nine electrons per one emitted Mössbauer γ-quantum, so it is preferable to register electrons; but at the same time this is more difficult due to the short absorption length of electrons in matter. So manipulations with electrons usually need high vacuum and electrostatic or magnetic optics. Energies and intensities of different radiations emitted in the de-excitation of the ^{57}Fe nucleus are shown in more detail in Table I. Intensities are indicated per one decay. From Table I it can be seen that besides X- and γ-rays we find four groups of electrons of different energies.

The first observation of the Mössbauer effect by conversion electrons was made in 1961 with a magnetic spectrometer.[11] Later, these studies resulted in the invention of the Mössbauer resonance counters.[12] Various applications of CEMS with different detectors but without LTDs were considered in the review.[13]

We proposed some possible schemes of the STJ Mössbauer resonance detectors in Ref. 14. Consideration of these possibilities requires a knowledge of the depth range of electrons in detector materials and related issues.[15] However, resonance detectors are not used in the present study.

The purpose of the present study is to observe the Mössbauer effect with the Nb-based STJ detector by registering the ^{57}Fe resonance electrons.

II. EXPERIMENTAL DETAILS

A silicon chip with five square-shaped detectors was attached with butyral phenolic glue to a copper substrate fastened by screws to the cold finger of the cryostat. The device was made at the Kotel'nikov Institute of Radio Engineering and Electronics of the Russian Academy of Sciences on the high-resistive Si substrate by using magnetron sputtering and photo lithography techniques. The photo and SEM images of the chip are shown in Figure 1. The vertical structure of detectors is from the bottom to the top Ti/Nb/Al/AlO_x/Al/Nb/NbN (layers thicknesses are 30/100/8/1/13/150/30 nm respectively, the role of each layer see in Refs. 6 and 16). The structure was made asymmetric deliberately in order to inactivate the bottom electrode by the Ti quasiparticle trap. It was done in order to decrease the collected charge from this electrode noticeably and to make use only of the signal from the top (active) electrode. There is a 100 nm of amorphous Al_2O_3 buffer layer between the detectors and the silicon. Two detectors with the sides of 100 and 150 micrometers were used in the present study, the first one being closer to the scatterer than the latter. We used the chip which was applied

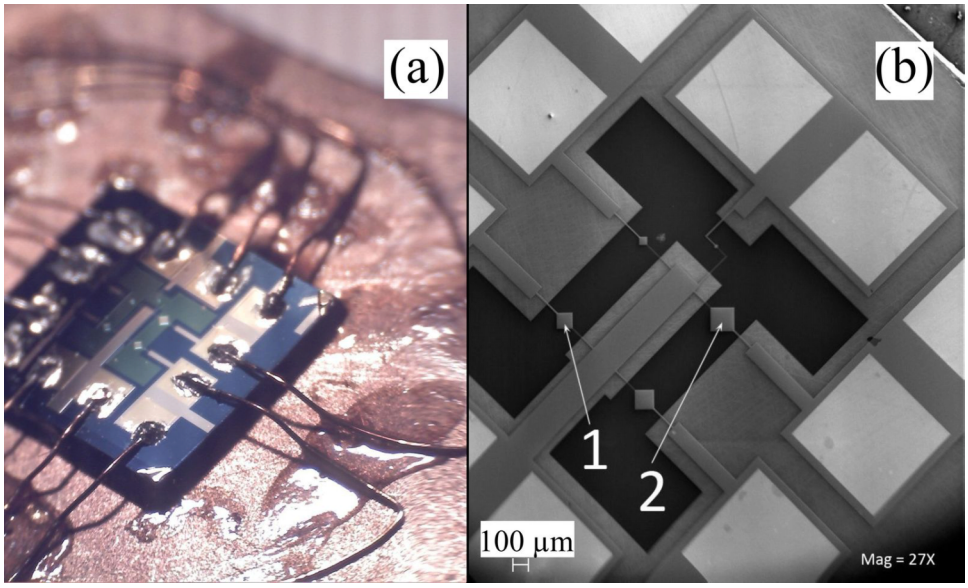

FIG. 1. (a) Photo and (b) electron microscope images of the chip with five square-shaped detectors. The detector sizes are 100 μm (1) and 150 μm (2).

earlier as an X-ray detector. Optimization of detector parameters for registration of electrons was not done.

The temperature was measured by a Ge resistance thermometer glued to the opposite side of the cold finger.

The Mössbauer source and the chip were placed perpendicularly to each other and the scatterer was placed at an angle of 45 degrees to both. The photo of the inner part of the experimental chamber and the sketch of experimental arrangement are shown in Figure 2. Wavy lines symbolize

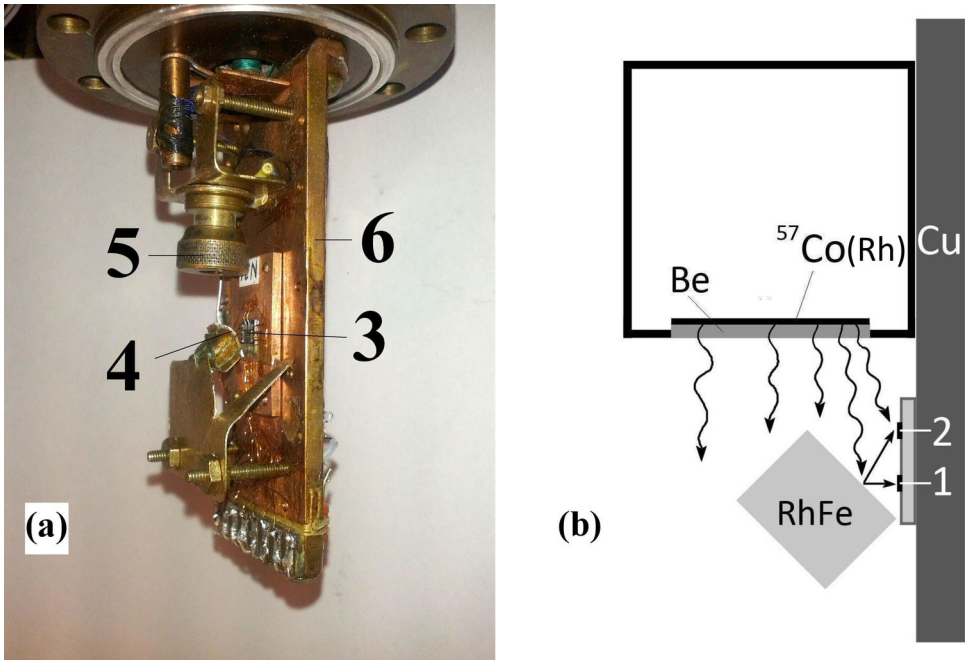

FIG. 2. (a) Photo of the inner part of experimental chamber with chip (3), Rh scatterer (4), simulant of the radioactive source (5) and cold finger (6); (b) sketch of the experimental arrangement with RhFe scatterer. The detector sizes are 100 μm (1) and 150 μm (2).

the gamma-quanta from the source and straight arrows show the difference in the distance from the scatterer point to the smaller (1) and the bigger (2) detectors. The diameter of the source active spot was 8 mm, the activity was ~20 mCi. The source, the scatterer and the detectors were in close vicinity to each other; all elements were in the static position.

Metallic Rh was the matrix for the ^{57}Co source. The same material was the main component for the alloy used as the scatterer, namely $Rh_{0.8}Fe_{0.2}$ enriched by the ^{57}Fe isotope. This particular choice allowed us to observe the effect at zero relative velocity of the source and the scatterer. No shields or diaphragms for incidental or scattered radiation were used. Thus all the detectors on the chip were permanently illuminated by direct and scattered radiation.

The magnetic field necessary for detector operation was applied in the detector's plane along the square diagonal. It suppressed the Josephson current and ensured the operation of the STJ in single quasiparticle mode. It was produced by a superconducting solenoid wound on a brass cylinder frame forming the experimental chamber. The chamber was filled with gaseous helium at lowered pressure and immersed in a pumped glass helium cryostat with a minimal temperature of nearly 1.4 K which we previously used for the study of the STJ detectors. The upper flange of the chamber with the leak proof indium seal is seen in Figure 2(a).

The magnetic moments of Fe in the $Rh_{0.8}Fe_{0.2}$ alloy do not align ferromagnetically at low temperatures and thus do not add to the solenoid magnetic field, which would be detrimental to the detector's operation. The antiferromagnetic nature of magnetic ordering for a given Fe concentration in these alloys was known long ago from macroscopic measurements[17] and a specific type of antiferromagnetic ordering was established in a study by Parfenova et al.[18] using the Mössbauer effect. A piece of the ingot of rectangular form (5*5*4 mm^3) with the scattering plane at 45 degrees to the chip surface was fixed in a holder (see Figure 2) 1 mm from the smaller and 2 mm from the bigger detector. (All values are approximate).

Earlier, we carried out experiments with X- and γ-rays filling the experimental chamber with a helium gas at a pressure of p ~0.3 bar at room temperature. This ensured a heat exchange, quick establishment of thermal equilibrium and a stable operation of the detectors. This quantity of helium is too high for experiments with electrons because they cannot reach the detectors without a significant loss of energy. (See estimations in section 3). For this reason, when carrying out experiments with electrons, we lowered the pressure of the heat exchange helium to the level which led to a moderate rise in temperature and a sufficient stability of the detectors operation.

Three kinds of experiments were carried out:

1. An X-ray detection experiment with the ^{55}Fe source: no scatterer; p ~0.03 bar of heat exchange He.
2. The main (Mössbauer) experiment with the ^{57}Co source: RhFe scatterer; p ~0.01 bar of heat exchange He.
3. A check experiment with the ^{57}Co source: pure Rh foil scatterer (without iron); p ~0.01 bar of heat exchange He for a direct comparison with the second experiment.

The tests of the detector's operation were carried out by measuring the current voltage characteristics (CVCs). In spectroscopic measurements, pulses from detectors were transmitted to a charge sensitive preamplifier at room temperature. Pulses after that could be fed into a digital oscilloscope or into an amplification path consisting of shaping and main amplifiers. Pulse height spectra from a multichannel analyzer and a series of pulses from the digital oscilloscope were recorded by a personal computer. All spectra were recorded with 13 min exposition in the magnetic field B=138 G.

The experimental equipment used in this study was essentially the same as in our previous investigations of the STJs as X-ray detectors.[5,6,16,19]

III. ESTIMATIONS OF THE MAXIMUM ELECTRON RANGES

We consider the propagation of electrons in matter bearing in mind the ideas given in the textbook by Balashov[20] and developed by Lukyanov,[15] Kanaya and Okayama[21] and Bakaleynikov.[22] According to these ideas, electron beam penetration in matter can be divided into two stages. In

TABLE II. The electron ranges R for the relevant energies in gaseous helium, Be window of the ^{57}Co source, the Nb absorber of the detector and the Rh scatterer.

E, keV	He[a], μm	Be, μm	Nb, μm	Rh, μm
14.3	460	3.1	1.1	0.78
13.6	430	2.9	1	0.73
7.3	140	0.97	0.39	0.27
5.5	80	0.6	0.26	0.18
4.0[b]			0.15	

[a]data are given for saturated He vapor at T = 1.4 K (p=$2.87 \cdot 10^{-3}$ bar), which allows us to make estimations for any pressure;.
[b]approximate energy of photoelectrons produced after absorption of Mn X-rays in Nb. It should be noted that the process of transferring energy to the absorber from the electron, which hits the absorber from outside, and from the electron produced inside the absorber, may be different.

the first stage, at a distance less than the isotropization length, the electron beam keeps its original direction despite energy loss. In the second stage, after the point of maximum dissipation of energy, the electrons in the beam "lose" their memory and their motion becomes diffusional. Here, the maximum electron range, R, may be considered as the sum of the isotropization length l and the radius r of the diffusion sphere: $R = l + r$.

We calculated the maximum electron ranges R in a continuous-slowing-down approximation (CSDA), using the stopping power from the eSTAR NIST database[23] for the materials of our interest (Table II). Similar results were obtained by calculating R according to the Kanaya-Okayama formulae[21] as given by Lukyanov in Ref. 15. (The difference is less than 25 %).

A considerable difference in the R value for helium and metals (more than two orders of magnitude) can be seen in the Table II. In metals $l < r$ and in the first approximation $R \approx r$. The situation for helium differs from that for metals: the isotropization length l is not short in comparison with the diffusion sphere radius r and cannot be neglected because now l is longer than r. The tendency of a fractional increase of l relative to r with a decrease in the atomic element number is clearly demonstrated in Ref. 21 (see Figure 14) and in Ref. 22 (Tables 1, 2, 3).

From our experimental conditions (pressure of heat exchange He at room temperature p~ 0.01 bar), we can estimate that the density of He is about 50 times less than that for saturated He vapor at T=1.4 K and we expect that the electron ranges should increase accordingly compared with the data from Table II. The electrons that have passed in helium the way less than R will transfer some of their energy to the detector and thus will be counted.

The maximum electron range in Be is more than two orders of magnitude less than the thickness of the Be window in the ^{57}Co radioactive source, so without doubt the conversion electrons do not escape from the source and cannot be registered by detectors.

The ranges for electrons of all energies in Nb exceed the thickness of the Nb absorber in the detector, so we expect to see rather peaks of partial but not full absorption. This disadvantage can be eliminated by optimizing the layer thicknesses of the detector.

The ranges in Rh for all electron energies do not exceed 1 micrometer. This is the depth limit for ^{57}Fe CEMS studies of Rh alloys. If we vary the thickness of the FeRh scatterer within this limit we will be able to change the relative contributions of X-ray fluorescence and conversion electrons to the detector signal.

IV. RESULTS

The current voltage curves measured before, between and after spectroscopic experiments revealed quite similar shapes in all three kinds of experiments and were identical to the CVCs measured in our previous experiments.[5,6,16]

The first experiment demonstrated that cooling at lowered pressure was sufficient and the detectors operated properly. We observed good current voltage curves (supplemental Figure S1[24]) and signals both of the active and inactivated electrodes in the pulse height spectrum (Figure S2[24]). For

the active electrode, the full width at half maximum of the Mn K_α line (5.89 keV) was less than 80 eV. (The contribution of electron noise was 60 eV, the intrinsic width was less than 60 eV). The signal (collected charge) of the inactivated electrode was nine times less than the active one. This allowed us to employ the region between these signals for a search for events in the active electrode.

The temperature rise was not higher than 0.02 K compared with the temperature in our previous X- and γ-rays experiments, and the detector operation was sufficiently stable. So the pressure was lowered by a factor of three in the second and the third experiments.

A comparison of the results of the irradiation of the RhFe alloy and the pure Rh foil as seen by the smaller (100 μm) detector is shown in Figure 3(a). For clarity, the pulse height spectrum in the case of RhFe was moved 400 counts upward relative to the Rh spectrum, and abscissa position of the most intensive peak was aligned. The spectrum in the case of Rh is the average of three measurements. The spectra were recorded at a T of about 1.4 K for detector bias near V_b = 0.8 mV. These spectra and all the other spectra presented in this work, were cut off on the left hand side at the level of the signal of the inactivated electrode. The check experiment spectrum is composed of Fe K_α and Fe K_β lines and a low charge line from the inactivated electrode. The spectrum of

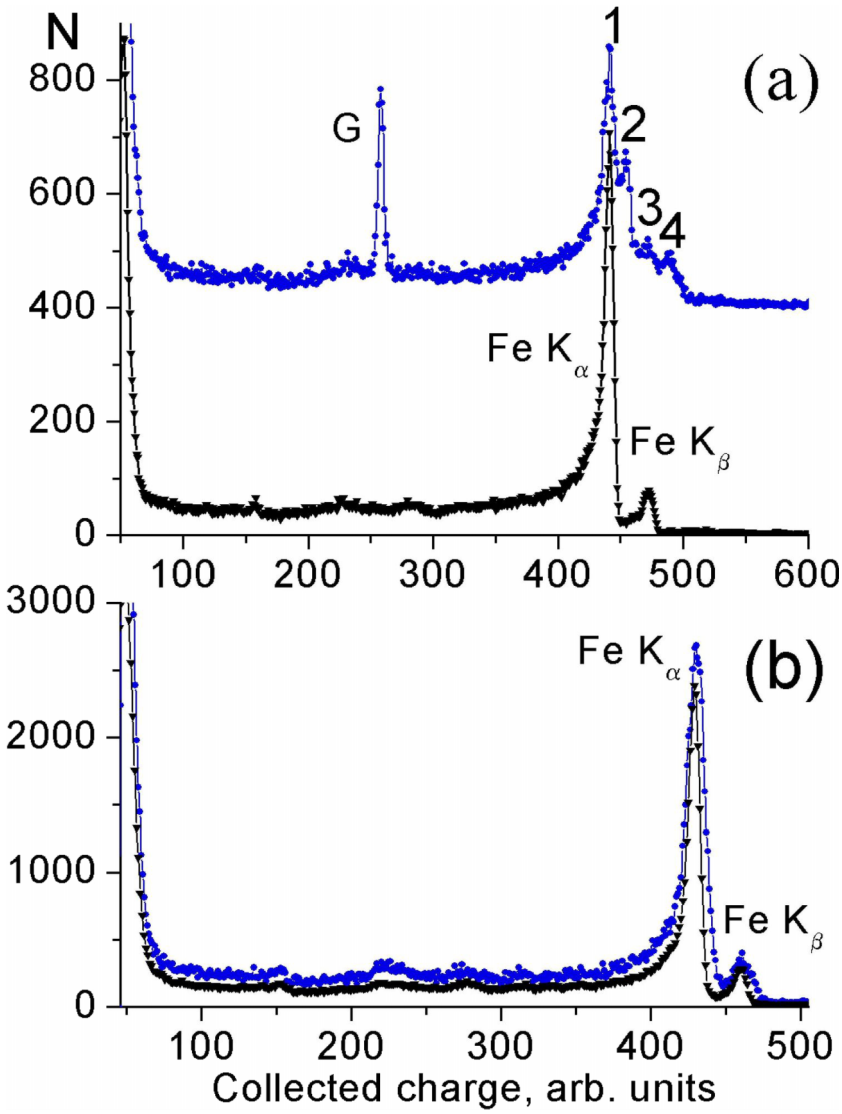

FIG. 3. Comparison of results of main experiment (blue circles) and check experiment (black triangles) for 100 (a) and 150 (b) μm detectors. 1,3 - Fe K_α, Fe K_β X-ray lines, 2,4 – resonant electron lines, G - a precise pulse height generator line. Peculiarities attributed to conversion and Auger electrons for RhFe and their absence for Rh scatterer can be seen.

the active electrode in the second experiment is composed of four rather than of two lines and a generator line G from a precise pulse height generator for charge calibration. We ascribe two additional lines in the spectrum (2,4 in Figure 3(a) to the signal from the electrons produced due to the nuclear gamma-resonance in the scatterer. Of course, this was not a full Mössbauer experiment with a velocity scale; rather it was a one-point measurement, corresponding to zero velocity in the Mössbauer spectrum.

The results for the bigger (150 μm) detector are shown in Figure 3(b). The abscissa position of the main peak was adjusted for coincidence. No pronounced peaks except Fe K_α and Fe K_β are observed. Besides, some line broadening and additional counts over the full spectrum in the RhFe alloy experiment can be seen. These spectra were recorded practically in the same conditions as previously. The spectrum in the case of Rh is also the average of three measurements.

Electron peaks for close-spaced 100 μm detector and absence of pronounced peaks for remote 150 μm detector should be noted.

The reproducibility of the results is illustrated in Figures 4(a) (nearby detector) and 4(b) (remote detector). Spectra recorded with a time interval of two hours for the 100 μm detector are shown by different symbols in Figure 4(a). A good correspondence can be seen, as both spectra

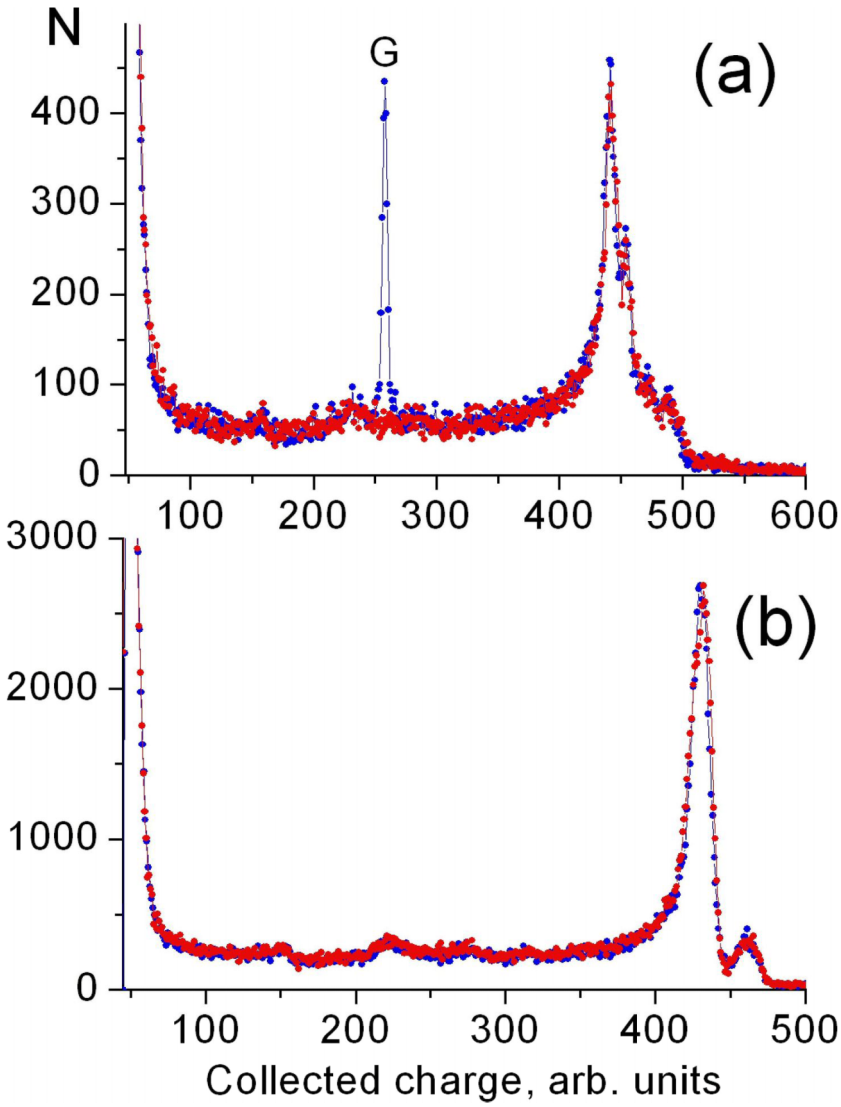

FIG. 4. Reproducibility of the results for closer to the scatterer (a, 100 μm) and more remote (b, 150 μm) detectors. Time intervals between measurements are two hours (a) and ten minutes (b).

demonstrate electron peaks. The results for the more distant 150 μm detector also show good reproducibility in Figure 4(b) where the symbols for the two subsequent experiments almost coincide. No sharp additional peaks are seen.

Our detectors are capable of registering 14.4 keV γ-line, not only Fe K_α and Fe K_β X-rays (Figure S3[24]).

V. DISCUSSION

First of all, a comparison of the second and the third experiments for the 100 μm detector clearly shows that we do observe NGR in the second experiment. The results for the two detectors separated by a distance of only 1 mm are quite different. We think that the reason for such a large difference is due to the character of electron proliferation in a low density He medium.

One can see the Fe K_α and K_β X-rays in all spectra shown in this paper. We cannot discriminate between the X- and γ-rays from the source and from the scatterer because no shields are used. We suppose that the two additional lines observed in our spectra overlapping with the lines of Fe K_α and K_β X-rays (Figure 3(a)) are lines from the 7.3 keV K conversion electrons and 5.5 keV Auger electrons which lost part of their energies on the way from the scatterer to detectors in the heat exchange helium. We do not consider L and M conversion electrons because their intensity is substantially below that of K and Auger electrons. We believe that the overlapping of X-ray and electron lines is accidental and can be changed in future experiments with varied exchange gas pressure and distance from the scatterer to detectors.

We see two possible explanations of the results for the bigger 150 μm detector. The first one is that the resonant electrons which reach the remote 150 μm detector, deposit an even smaller part of their initial energy than in the case of the closer to the source 100 μm detector. Their lines can be almost in the same place as the X-ray lines. Overlapping of broader electron lines with more narrow X-ray lines can result in the broadening of the observed lines rather than in the emergence of extra peaks (Figure 3(b)).

The second one is connected with the relative dimensions of detectors and the diffusion sphere. We consider every point of the scatterer as the origin of electron beams in all directions. If the electrons were in a vacuum, they would move along cylindrical helix lines with radii determined by the velocity component perpendicular to the field, and the pitch would be determined by a velocity component parallel to the field. In helium, every collision changes the velocity components, but in general the two-stage character of the electron motion does not change. When the detector encounters the electron beam in the first stage, it produces an absorption peak at the energy depending on the fraction of energy lost by the beam on the way from the scatterer to the detector. This seems to be the case for the first 100 μm detector. When the second stage of the electron beam motion is realized, a detector produces single counts corresponding to electrons of different energies, depending on the detector's position in the diffusion sphere. This is because the area of our detectors is significantly less than the cross section of the diffusion sphere when $r \sim 1$ mm in helium. It is likely that this second stage can be realized for the 150 μm detector and explains the extra counts in the whole spectrum Figure 3(b).

The efficiency of proportional counters for the 14.4 keV gamma line compared with that for the 6.4 keV X-ray is usually of the same order or several times less. The efficiency of our detector differs by an order of magnitude for these energies. Thus, the background from the 14.4 keV line is reduced accordingly. Furthermore, the background from the Compton scattering of the 14.4 keV gamma line is also small due to thinness of our detectors. These two examples show that a low efficiency of a thin film superconductor detector, which is usually considered to be a drawback, may play a positive role.

Considering possible future applications of our results, we see that they may be compared with the CEMS results which use specimens placed inside low temperature helium proportional counters.[25,26] It can be seen directly from our spectra, that the electron line resolution of our detectors is of the same order as the X-ray line resolution, which far exceeds the resolving power of proportional counters. From this point of view, we expect that the STJ detectors have advantages over helium proportional counters for the CEMS.

We believe that our experimental assembly of a detector and a scatterer placed in chamber filled with gaseous helium in the presence of an applied magnetic field demonstrates the combination of properties appropriate for proportional counters with resonance absorbers and also for magnetic electron spectrometers. This allows considering possible applications of the STJ detectors for registering with moderate resolution any type of electrons (not only resonance ones). We think that the STJ detectors will find their place in the field of surface and thin film analysis, considered in the excellent book by Feldman and Mayer[27] written when the STJ detectors were in the early stage of their development.

VI. CONCLUSIONS

We applied a specially selected pair of the source ^{57}Co(Rh) and the RhFe scatterer to observe the Mössbauer effect at zero relative velocity. We believe that the results we obtained confirm the registration of resonant electrons, and thus the observation of the nuclear gamma resonance with the Nb STJ detector.

We demonstrated the detection of the resonant electrons, the 14,4 keV γ-line and the Fe K_α and Fe K_β X-rays with our detectors. It is thus possible to use the STJ detectors for registering the NGR for all kinds of radiation: resonant electrons, γ-rays and X-rays.

We considered the proliferation of electrons in helium, and proposed the reasons why the lines of resonant electrons were observed for the detector close to the scatterer but were smeared out for the detector only 1 mm further away.

Our result is just the first step in using the STJ detector for NGR research. The plan for future experiments is straightforward: it is necessary to vary gas pressure and scatterer-detector distances to check our explanation of the difference in the results for the two detectors. Then one should do a full-scale Mössbauer experiment to measure the velocity spectrum using another cryostat with windows transparent for the Mössbauer radiation. The radioactive source should be placed outside while the scatterer and detector should be inside the cryostat. We hope that experiments in this geometry using the STJ detectors may be applied for depth selective low-temperature Mössbauer spectroscopy.

ACKNOWLEDGMENTS

The authors are grateful to Ms. H. M. Jones for editing the English and to Dr. Yu.V. Orlov for critical reading of this manuscript. We also would like to thank Dr. S.K. Godovikov for fruitful discussions, Dr. M.A. Timofeev for the SEM investigation of our detectors and also Dr. A.L. Erzinkyan for providing us with the specimen of the RhFe alloy.

This study was supported in part by the Russian Foundation for Basic Research (grant 09-02-01402), and by the Ministry of Education and Science of the Russian Federation (grants 14.607.21.0100 and HIII-4871.2014.2).

[1] Chr. Enss (Ed.), *Cryogenic Particle Detection 2005*, Topics Appl. Phys. (Springer-Verlag, Berlin, Heidelberg, 2005), Vol. 99, p. 500.
[2] P. Lerch and A. Zehnder, *Quantum Giaever Detectors: STJ's.* Chapter in Ref.1 p.217–267.
[3] G. H. Wood and B. L. White, Appl. Phys. Lett. **15**, 237 (1969).
[4] S. Friedrich, J. Low Temp. Phys. **151**, 277 (2008).
[5] M.G. Kozin, I. L. Romashkina, S. A. Sergeev, L. V. Nefedov, V. P. Koshelets, and L. V. Filippenko, Bulletin of the Russian Academy of Sciences: Physics **71**, 1302 (2007).
[6] M. G. Kozin, I. L. Romashkina, S. A. Sergeev, L. V. Nefedov, V. P. Koshelets, and L. V. Filippenko, Instruments and Experimental Techniques **49**, 868 (2006).
[7] P. H. Videler, N. Rando, P. Verhoeve, A. J. Peacock, S. Lemke, J. Martin, R. Gross, R. P. Huebener, and J. M. Lumley, Proc. SPIE **2280**, 352 (1994).
[8] P. E. Wagner, J Phys (Paris) Coloq **37**, C6-673 (1976).
[9] G. N. Belozerskii, *Mössbauer Studies of Surface Layers*, Studies in Physical and Theoretical Chemistry Series (Elsevier Science, 1993), Vol. 81.
[10] National Nuclear Data Center, Brookhaven National Laboratory. NuDat 2.6. Decay Radiation Search. See http://www.nndc.bnl.gov/nudat2/dec_searchi.jsp.
[11] K. P. Mitrofanov and V. S. Shpinel, JETP **13**(3), 686 (1961).

[12] K. P. Mitrofanov, N. V. Illarionova, and V. S. Shpinel, Pribory i Tekhnika Eksperimenta **No.3**, 49 (1963) in Russian.
[13] K. Nomura, Y. Ujihira, and A. Vertes, Journal of Radioanalitycal and Nuclear Chemistry **202**(1-2), 103 (1996).
[14] M. G. Kozin and I. L. Romashkina, *Abstracts of XI International Conference on Mössbauer Spectroscopy and its Applications* (Ekaterinburg, Russia, 2009), p. 180.
[15] F. A. Lukyanov F A, E. I. Rau, and R. A. Sennov, Bulletin of the Russian Academy of Sciences: Physics **73**, 441 (2009).
[16] M. G. Kozin, I. L. Romashkina, S. A. Sergeev, L. V. Nefedov, V. A. Andrianov, V. N. Naumkin, V. P. Koshelets, and L. V. Filippenko, Nuclear Instruments and Methods in Physics Research Section A: Accelerators, Spectrometers, Detectors and Associated Equipment **520**(1–3), 250 (2004).
[17] N. P. Grazhdankina, Soviet Physics Uspekhi **11**(5), 727 (1969).
[18] V. P. Parfenova, N. N. Delyagin, A. L. Erzinkyan, and S. I. Reiman, Physics of the Solid State **42**(8), 1465 (2000).
[19] V. A. Andrianov, P. N. Dmitriev, V. P. Koshelets, M. G. Kozin, I. L. Romashkina, S. A. Sergeev, and V. S. Shpinel, Nuclear Instruments and Methods in Physics Research Section A: Accelerators, Spectrometers, Detectors and Associated Equipment **444**(1–2), 19 (2000).
[20] V. V. Balashov, *Stroeniye veshestva (Structure of matter)* (Moscow State University Publisher, Moscow, 1993), p. 216 in Russian.
[21] K. Kanaya and S. J. Okayama, Phys. D: Appl. Phys. **5**, 43 (1972).
[22] L. A. Bakaleinikov, E. Yu. Flegontova, K. Yu. Pogrebitskii, H.-J. Lee, Y.-K. Cho, H.-M. Park, and Y.-W. Song, Technical Physics **46**(7), 796 (2001). Translated from Zhurnal TekhnicheskoI Fiziki **71**(7), 14 (2001).
[23] M.J. Berger, J.S. Coursey, M.A. Zucker, and J. Chang, ESTAR, PSTAR, and ASTAR: Computer Programs for Calculating Stopping-Power and Range Tables for Electrons, Protons, and Helium Ions (version 1.2.3). National Institute of Standards and Technology, Gaithersburg, MD. [Online*, 2014, April, 17*]. See http://physics.nist.gov/PhysRefData/Star/Text/ESTAR.html.
[24] See supplementary material at http://dx.doi.org/10.1063/1.4942429 for current voltage curves for the 100 μm detector (Figure S1); pulse height spectrum measured with the ^{55}Fe source for this detector (Figure S2) and pulse height spectrum measured with the ^{57}Co source for bigger (150 μm) detector and the Rh foil scatterer (Figure S3) in the logarithmic scale for a higher energy diapason than in Figure 3(a).
[25] T. Fujii, R. Katano, S. Ito, and Y. Isozumi, Bull. Inst. Chem. Res. Kioto Univ. **68**(2), 110 (1990).
[26] S. Masaoka, R. Katano, S. Kishimoto, and Y. Isozumi, NIM B **171**, 360 (2000).
[27] L. C. Feldman and J. W. Mayer, *Fundamentals of surface and thin film analysis* (North-Holland New-York Amsterdam, London, 1986).